ARTICLE

Deterministic Positioning of Few Aqueous Colloidal Quantum Dots†

Received 00th January 20xx,
Accepted 00th January 20xx

DOI: 10.1039/x0xx00000x

Muhammad Tegar Pambudi[#,a,b,c], Deepshikha Arora*[,#,b], Xiao Liang[d], Basudeb Sain[b,e], Anupama Sargur Ranganath[b], Matthew R. Chua[a], Cam Nhung Vu[b], Golnoush Zamiri[b], Md. Abdur Rahman[b], Hilmi Volkan Demir*[,d,f,g], Joel K. W. Yang*[,b], Lu Ding*[,a]

Emerging quantum technologies that critically require the integration of quantum emitters on photonic platforms are hindered by the control over their position, quantity, and scalability. Herein, we describe a facile strategy to deposit aqueous silica-coated quantum dots (QDs) in a template of polymethyl methacrylate (PMMA) nanoholes that leverages on saturated ethanol vapor drop-casting and subsequent lift-off of the template. Ethanol vapor incorporation into water droplets during the drying process reduces the meniscus contact angle, which increases capillary forces and enhances particle confinement within the pinning contact region. Furthermore, induced Marangoni flow controls the particle transport dynamics inside the droplets making large-scale deposition possible. Controlling the hole diameter of the template demonstrates changes in the number of QDs per hole, which is consistent with the Poissonian distribution with the best results of ~40% single-particle yield from a ~80% total site occupancy. This method employs a simple setup, eliminating the need for intricate optimization, yet offers the potential for deterministic patterning within complex photonic platforms.

Introduction

Quantum emitters integration with photonic platforms paves the way in emerging quantum technologies[1,2] and facilitating essential investigations into light-matter interactions[3–9]. In a photonic cavity with small mode volume, e.g., deep sub-wavelength localization of plasmonic cavity[3,4] and high Q-factor dielectric photonic resonators[5,6], emitter positioning in nano-scale precision is crucial to enhance emitter-cavity coupling. Besides, controlling the position in such a specific arrangement or number of the emitters is both interesting and essential for achieving coherent interactions in super-radiance or super-fluorescence[7–9].

While several sources of emitters have already been incorporated with photonic platforms, e.g., single atoms[10], self-assembled quantum dots (QDs)[11–14], color centers in diamonds[15,16], and defect centers in 2D transition metal dichalcogenides (TMDCs)[5,17], the flexibility and scalability in controlling the number and position of these emitters are often limited. On the other hand, colloidal semiconductor nanocrystals, i.e., colloidal QDs, are widely explored due to their

[a.] Institute of Materials Research and Engineering (IMRE), Agency for Science, Technology and Research (A*STAR), 2 Fusionopolis Way, Innovis #08-03, Singapore 138634, Republic of Singapore
[b.] Engineering Product Development, Singapore University of Technology and Design, Singapore 487372, Singapore
[c.] School of Electrical and Electronic Engineering, Nanyang Technological University, Singapore 639798, Singapore
[d.] LUMINOUS! Center of Excellence for Semiconductor Lighting and Displays, The Photonics Institute, School of Electrical and Electronic Engineering, Nanyang Technological University, Singapore 639798, Singapore
[e.] Department of Atomic and Molecular Physics, Manipal Academy of Higher Education, Manipal, Karnataka 576104, India
[f.] Division of Physics and Applied Physics, School of Physical and Mathematical Sciences, Nanyang Technological University, Singapore 637371
[g.] UNAM-Institute of Materials Science and Nanotechnology, The National Nanotechnology Research Center, Department of Electrical and Electronics Engineering, Department of Physics, Bilkent University, Bilkent, Ankara, 06800, Turkey
* deepshikha_arora@sutd.edu.sg
* hvdemir@ntu.edu.sg
* joel_yang@sutd.edu.sg
* dingl@imre.a-star.edu.sg

† Electronic Supplementary Information (ESI) available: Particles count and percentage, absorbance and photoluminescence spectra of colloidal QDs solution, photoluminescence setup for QDs on substrate. See DOI: 10.1039/x0xx00000x

# These authors made equal contributions to this works

unique electrical and optical properties. These nanocrystals encompass adjustable emission wavelengths, with the potential to extend into the telecom range[18–20], room-temperature stability[21], and their notable antibunching phenomena[22]. Furthermore, colloidal QDs are amenable to solution processing, providing substantial scope for seamless deterministic integration into various material platforms and nanocavities. Various assembly techniques have been explored, aiming to achieve precise positioning, high process controllability, and scalability. Numerous studies have demonstrated the placement of metal nanoparticles (NPs) and polymeric colloidal units with high precision and yield[23–25]. However, there remains a significant gap in the development of analogous techniques for colloidal QDs probably due to their small size and intricate surface chemistry[22,26].

Various strategies have been extensively investigated for the deposition of QDs, primarily employing trap templates prepared through high-resolution electron beam lithography (EBL). Positioning of QDs into the traps then relies on techniques such as electrostatic interaction[27,28] and capillary forces[22,29–31]. The electrostatic interaction technique involves pre-growing traps with positive surface charges on a negatively charged substrate. QDs particles, with matching negative surface charges, are then attracted to the traps while repelled by the substrate. It reports the near-unity single particle occupancy for a typical particles size greater than 150 nm. This method works perfectly if the surface charge orthogonality exists between the traps and the particles/substrate. However, common high-index dielectric materials for making photonic structures such as TiO_2, Si_3N_4, and SiC might have iso-electric point (IEP) at low pH[32], so that they have negative surface charges same as that of the QD particles. Therefore, the applicability of this technique in photonic integration is limited. The capillary force techniques include Langmuir Blodgett[33] and doctor blade-like[22,29,34] approaches, achieving a typical total site occupancy above 70%, while single particle yield of ~75% is once reported using silica-cladded QDs of diameter 90 nm. This method requires intricate setups with moving parts to manipulate the particles into the traps, as well as precise controlling of the substrate temperature and dew points within the setup environment. On the contrary, drop-casting method is much simpler for non-functionalized particles/substrates/traps and shows potential in quick and easy implementation of meniscus capillary force for deterministic positioning[30,31,35]. Yet, the reported single particle yield is ~30% with the best total site occupancy is 60%. Therefore, as the controlled placement of QDs is remains a challenge, the scalability and reproducibility are yet to be fully elucidated.

In our study, we present a straightforward method that leverages only the drop-casting process onto a poly(methyl methacrylate) (PMMA) template for aqueous silica-coated QDs. The drying process takes place within a saturated ethanol vapor environment, which facilitates large-area uniform mass deposition of the QDs promoted by Marangoni flow and enhances the capillary force due to modified wetting properties of the colloidal droplet. A final lift-off step is employed to remove unwanted QDs from outside the intended area, achieving clean surface which is useful for photonic integration. Our experimental results demonstrate a single-particle yield of 40%, with total site occupancy reaching 80%, wherein the number of QDs and yield can be controlled by varying the size of the hole template. We note that the hole size needs to be at least 3 to 4 times larger than the QD size to achieve high single-particle yield. Leveraging large-sized QDs controlled by silica coating, the template size aligns with typical photonic platforms ith visible spectrum resonance thus enabling simple one-step lithographic integration.

Result and Discussion

The schematic of the patterning process flow chart is shown in **Figure 1(a)**. First, PMMA hole templates are patterned with EBL on a silicon (Si) substrate, SEM image shown in **Figure 1(b)**. Holes with different diameter was prepared as the number of particles deposited is expected to be dependent on the particle size. Second, a droplet of aqueous-based silica-coated QDs with an average size of 34.1 ± 3.4 nm are drop-casted on the template. The sample is then left to dry in a saturated ethanol vapor environment. Third, a uniform thin film of QDs is formed on the top of the template. In the final lift-off process, the PMMA template is dissolved in warm acetone then reveals the deterministically positioned QDs, SEM image shown in **Figure 1(c)**. See details of the patterning condition in Experimental Method.

In our study, the patterning process utilizes silica-coated quantum dots (QDs), offering three distinct advantages. Firstly, the silica shell increases the effective size of the QDs. It is well-established that the deposition yield is influenced by the ratio of template size to QDs size, where results from various method, i.e. drop-casting and Langmuir-Blodgett, needs the hole size to be 2-4 times larger than the QDs size[30,31,33]. The extension of the effective size simplifies the fabrication process of templates, particularly when employing electron beam lithography (EBL), eliminating the need for intricate optimization of very small hole features.

Secondly, silica-coating facilitates the phase transfer of QDs from organic solvents to water. The choice of solvent is pivotal, especially in mass deposition techniques such as the drop-casting process. Numerous studies have demonstrated the ability to control deposition patterns[36–38], whether particles are concentrated at the edge, center, or in between the drop-casted region. Our approach, inspired by Ref. [37], utilizes saturated ethanol vapor to ensure the uniformity and scalability of the deposited film of particles dispersed in water. This method enhances control over the deposition process, particularly in terms of reproducibility.

Thirdly, silica-coating is a common practice across various classes of nanoparticles, including perovskite[39], plasmonic[40], and up- and down-conversion nanoparticles[41]. Beyond phase transfer, silica-coating serves to protect their physical properties from environmental factors. Consequently, our method extends beyond QDs, offering the potential to deterministically position various core materials with silica-

coating in an aqueous phase. This versatility underscores the broader applicability and utility of our approach in nanoparticle patterning and integration.

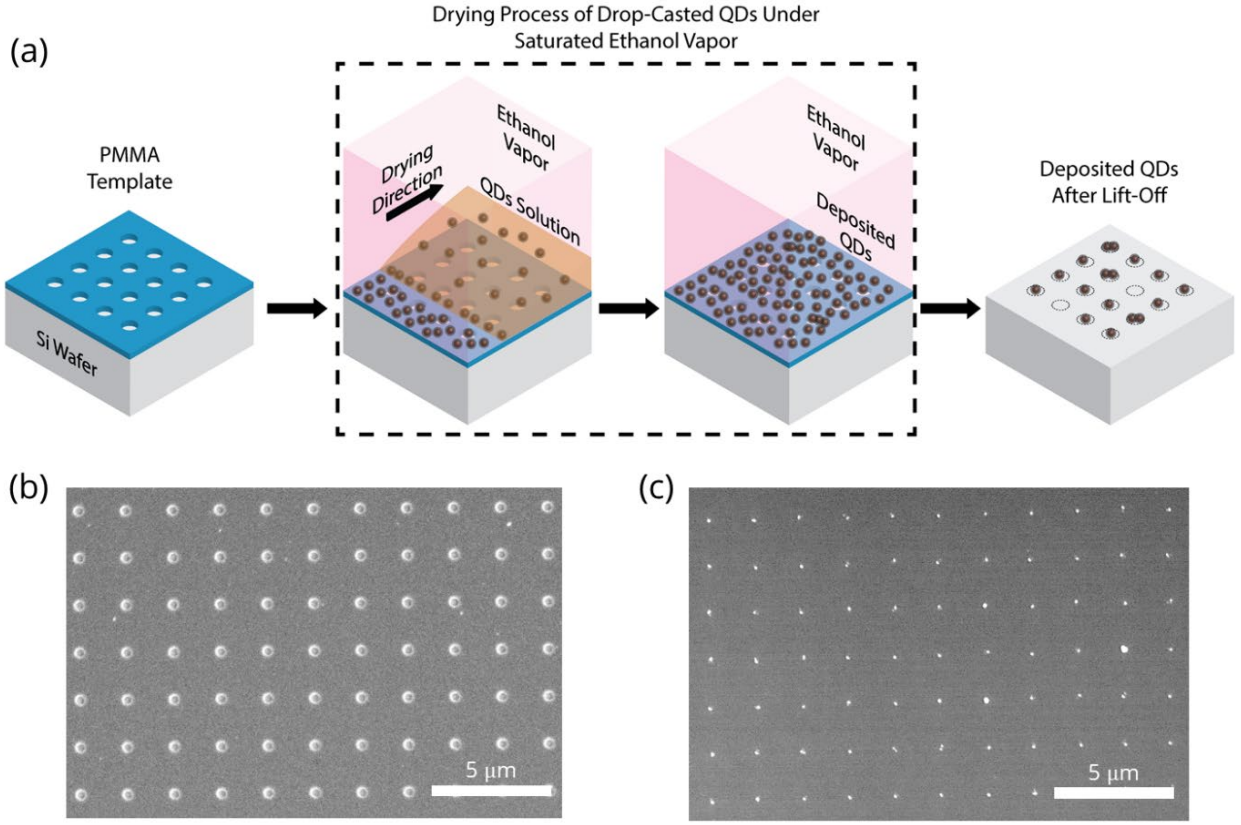

Figure 1. (a) Illustration of the process flow. PMMA template is made by EBL on Si substrate. QDs are deposited by drop-casting and dried under saturated ethanol vapor environment followed by template lift-off. SEM images are shown for **(b)** PMMA template and **(c)** deposited QDs after lift-off.

Using the described method, herein we report the average result of 3 samples. Each sample employed a PMMA template featuring circular hole arrays with a thickness of approximately 60 nm and hole diameters ranging from 130 to 190 nm. **Figure 2** shows the statistical analysis averaged from all samples, see **Table S1** for raw particle count data and **Table S2** for count percentage for each sample. **Figure 2(a**) shows full statistics of the site occupation as a function of hole diameters and number of particles in the left column and the corresponding SEM images on the right, SEM image taken from sample #3.

We observed high site occupancy rates exceeding 80% for hole diameters ranging from 130 nm upwards, progressively increasing towards near unity with larger holes. The single-particle yield at a hole diameter of 130 nm is reaching 42% with the remaining sites accommodating up to 3 particles per site. However, as the hole diameter increased, the single-particle yield decreased, with larger diameters only accommodating a maximum of 6 particles per site, as seen with 190 nm holes.

In sample #3, featuring smaller hole diameters of 110 nm (not shown here), the total site occupancy dropped to 43%, with a single-particle yield of 30%. Notably, the calculated size ratio between the hole and QD diameter suggests that the optimum single-particle yield falls within the range of 3.1 to 3.7, consistent with previous studies. However, it's important to acknowledge that a high ratio results in significant placement deviation of the QDs. For instance, with respective hole and QD diameters of 130 nm and 35 nm, the deviation can reach up to ±50 nm. Therefore, achieving precise QD placement necessitates smaller particle sizes to accommodate higher precision, particularly in structures such as photonic cavities with small volume modes.

The particle deposition processes with drop-casting[30,31] and Langmuir-Blodgett[33] shown to have typical Poissonian distribution as,

$$P(x) = \frac{\lambda^x}{x!}\exp(-\lambda), \qquad (1)$$

where $P(x)$ is the probability (yield) of x number of particles deposited and λ to be the expected rate of occurrences. We fitted the data with a Poissonian distribution where the λ-value is proportional to the hole diameter with the smallest of 1.4 at a hole diameter of 130 nm, i.e. on average 1.4 QDs deposited in each hole. The Poissonian distribution also indicates that the highest probability of single particles from random, discrete, and independent events is limited at $1/e$ or ~37% which matches fairly with our results. The same statistics are done for other hole diameters and with SEM images showing QDs with different occupation numbers. The λ-value increases with the size of the holes, see **Figure 2(b)**. It is possible to get a smaller λ-value close to one with a smaller hole size, however, it will

also reduce the total site occupation which then also reduces the single-particle yield.

In this study, to control the particle deposition over a large area with a uniform mass deposit, we introduce a saturated ethanol

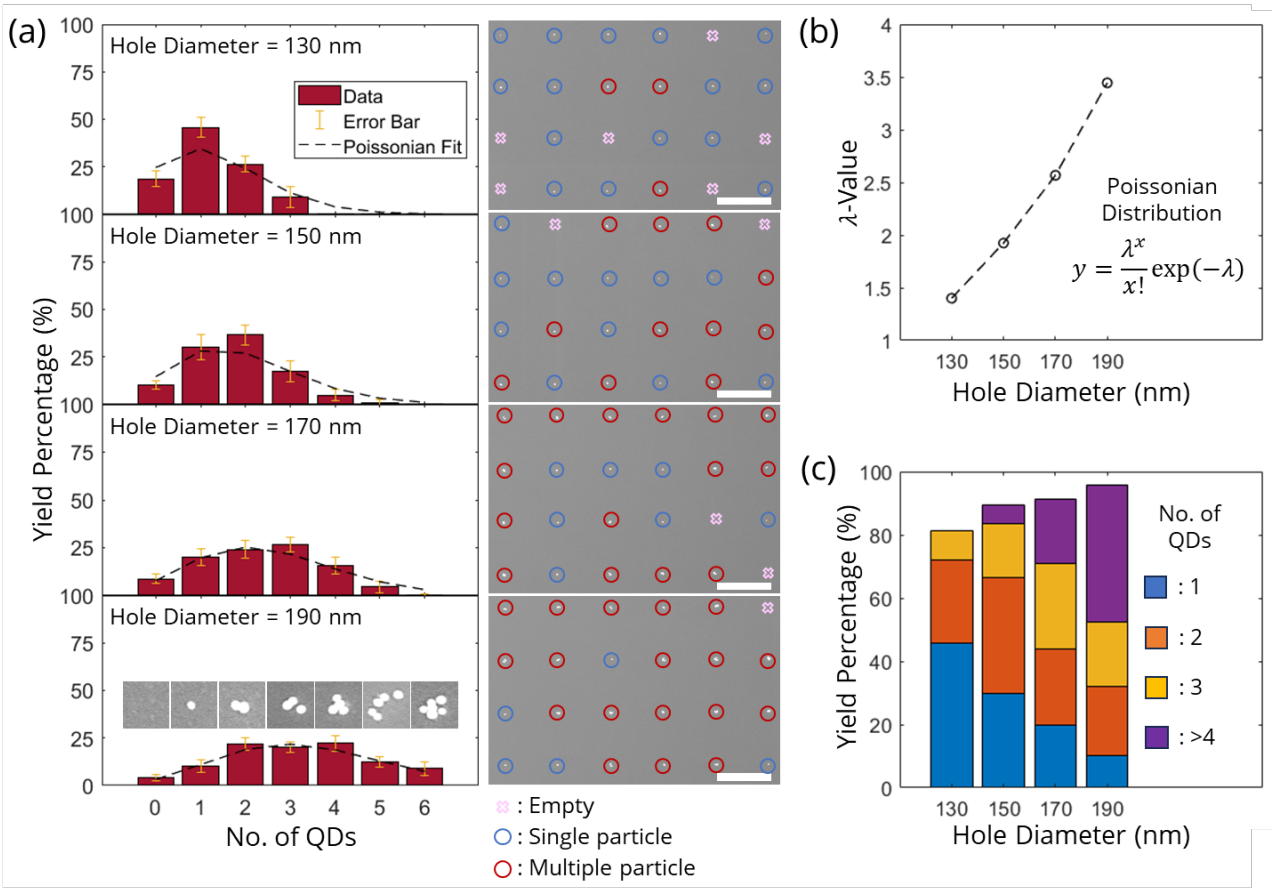

Figure 2. (a) Average QDs distribution from 3 different samples for hole diameter range from 130 – 190 nm with their respective SEM images in an array with the pitch of 2 µm showing sites which empty and filled with either single or multiple particles. All SEM images herein are with the same magnification and share the same scale bar of 2 µm. **(b)** λ-value taken from the Poissonian model fitted into the QDs distribution plot. **(c)** Stacked-bar plot of QDs distribution versus hole diameter from the same statistical data.

Figure 2(c) plots the averaged particle counts for 1, 2, 3, and more than 4 particles as a function of hole diameter as an example which shows the total occupancy yield with increased diameter. It should be noted that using a larger hole size also spreads the distribution with a larger deviation. By this means, such a method is only optimum to prepare high-yield single particles but control over the narrow distribution of a few particles will be harder.

The choice of solvents is crucial as it will dictate the mass transport phenomena and their respective deposition mechanism. In **Figure 3(a,c)**, we show that drop-casting of an aqueous QD droplet at ambient environment results in a "coffee-ring" pattern indicated by high mass deposit at the edge. Illustration described the phenomenon in which the particle flux is being directed towards the pinning contact region which is then later deposited as the droplet dries. Furthermore, it was later known that the formation of the ring pattern is due to the suppressed particle flux back to the bulk region[36,42]. By this means, particle concentration at the pinning contact region will be high at the initial drying process, thus high mass deposit, and gradually decreases as the process continues.

vapor environment during the drying process of an aqueous QDs droplet. In this environment, a phenomenon called Marangoni flow is caused by the non-uniform absorbed ethanol concentration and evaporation rate along the droplet surface where it induced flows into the pinning contact and back-flow into the liquid bulk[37]. This particle dynamic leads to the formation of a uniform deposition of mass across the substrate, see **Figure 3(b,d)**.

Another phenomenon shown during the experiment is the reduced contact angle due to the wetting properties modification as the ethanol absorbs into the water droplet, see **Figure 3(e,f)**. The contact angle from the water droplet at ambient pressure seems to not change significantly and stays at ~70°. However, by the time we put the droplet inside the saturated vapor environment, the contact angle already reduced significantly to ~44° and continued to be reduced further to ~32° in under 30 seconds. The wetting properties modification can be explained by the formation of the water/ethanol binary mixture within the droplet. As the ethanol

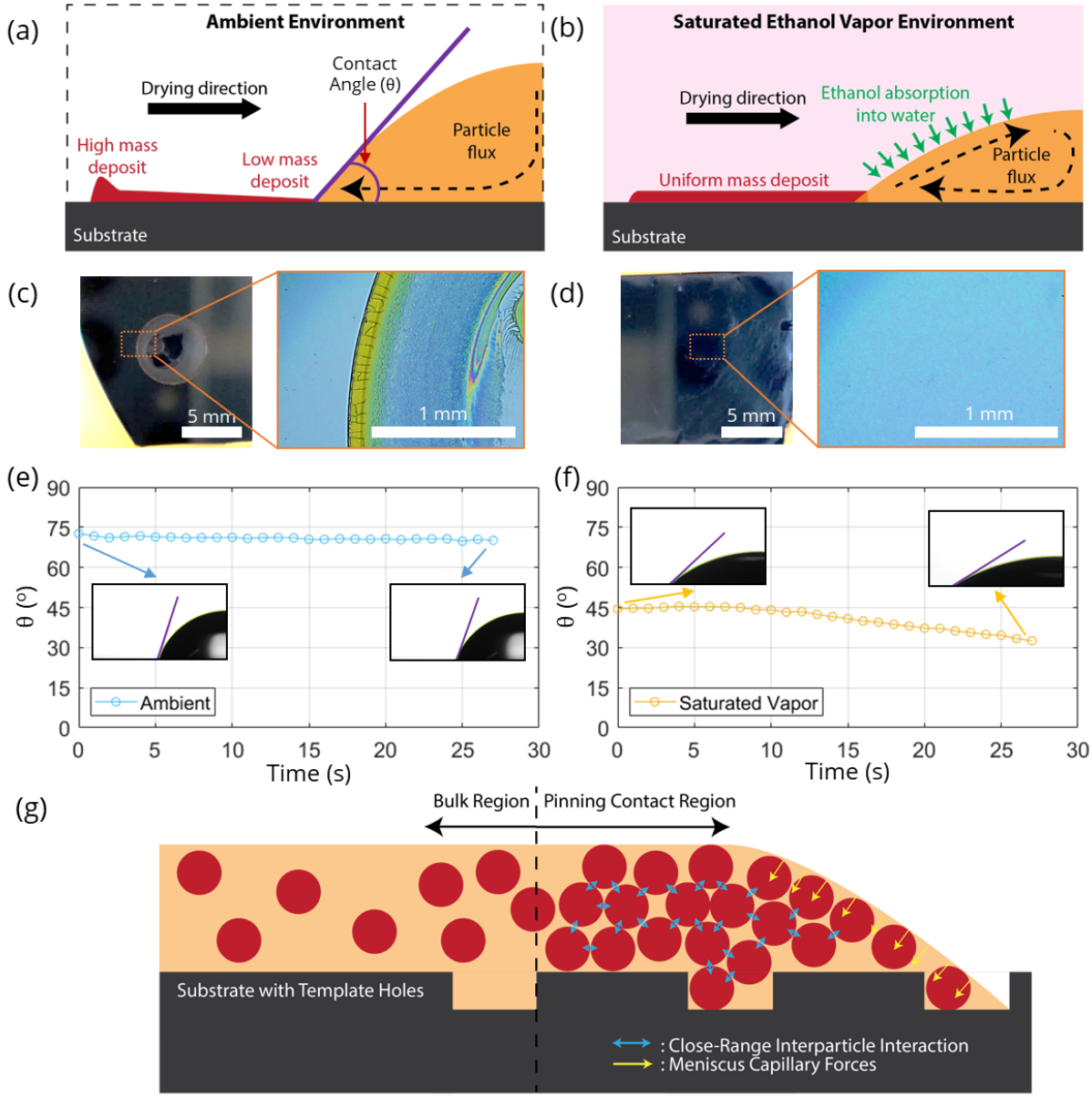

Figure 3. Illustration of particle deposition on a macro-scale in **(a)** ambient and **(b)** saturated ethanol vapor. Photograph and zoomed-in optical microscope images of the dry QDs on PMMA film on Si substrate at **(c)** ambient and **(d)** saturated ethanol vapor. Room temperature contact angle measurement of a sessile pure water droplet on flat PMMA film on Si substrate at **(e)** ambient and **(f)** saturated ethanol vapor. **(g)** Schematic on the three-phase contact confinement mechanism for template-assisted particle deposition.

concentration increases over time until reaching saturation in the droplet, the contact angle will reduce.

For the case of the drop-casting deposition method, we can deduce 2 main driving forces for which particles can go into the template: (1) meniscus capillary forces and (2) close-range interparticle interaction, see **Figure 3(f)**. First, capillary forces induced at the pinning contact which intersected with the meniscus proportional to $\cos\theta$, with θ is the contact angle of the fluid on substrate[43]. Thus, larger capillary forces are in favor of drying droplets in saturated ethanol vapor with a significantly reduced contact angle. For the second driving force, a simulation study where interparticle forces are considered shows that it is possible for the particles to be deposited into the template far away from the pinning contact meniscus due to the interparticle close-range repulsive interaction[43–45]. Also practically, by the presence of the short-range interparticle interaction, an effective hopping interaction from meniscus capillary force acted at the particle near the liquid/vapor interface can be felt by the particle far away from the interface. By these means, we considered a deposition mechanism in which attributed the meniscus line and/or particle-particle confinement. Thus, respectively, the driving force is provided from the capillary force and/or short-range interparticle repulsive force.

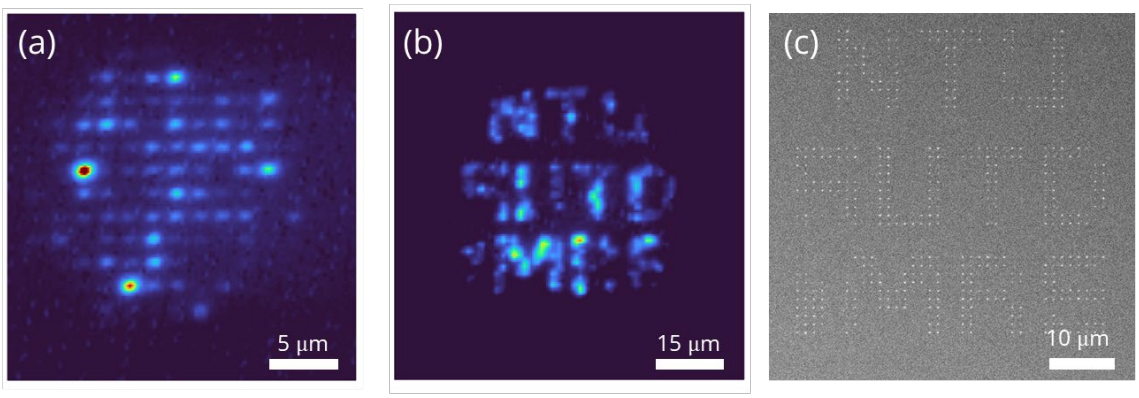

Figure 4. Wide field PL image with CW laser excitation at 488 nm from **(a)** an array of QDs deposited with template hole diameter of 150 nm and pitch 2 µm, taken with 50x (NA 0.55) objective lens, and **(b)** pattern of our collaborating institutions as a proof of concept prepared with template hole diameter of 150 nm, taken with 20x (NA 0.45) objective lens. **(c)** SEM image from collaborating institutions pattern.

At this point, we need to understand that the capability of controlling the dynamic concentration and its relationship with the provided driving force is important for large-scale positioning. Using an ambient environment, the non-uniform particle flux at the pinning contact region, ring-pattern mass deposit, and large contact angle might not be suitable for the large-scale method. Whereas in saturated ethanol vapor, the particle dynamics and wetting properties modification can provide the solution for these issues.

To check the robustness of the QDs through the deposition process, we used photoluminescence (PL) microscopy to check the emission signal. **Figure 4(a)** shows the PL maps of QDs deposited on an array with a pitch of 2 µm, featuring a hole size of 150 nm, to achieve a high total yield while maintaining the deposition of few particles. The map retrieved for the area of 26 x 26 μm^2 which is defined by the laser spot size, see **Figure S2** for detailed information. High-intensity signal corresponds to the QDs position where signal differences between sites might come from the different quality of individual QDs and/or number of particles deposited. It is important to maintain the laser power and integration time as there is a trade-off between signal-to-noise ratio and QD stability, e.g., photo-bleaching and blinking. We use the laser power density with a 50x (0.55 NA) objective lens of 10.1 W/cm^2 by expanding the laser beam and distributing the power, see **Figure S2** for details on PL measurements. Furthermore, QDs can be positioned on specific patterns of the template. **Figure 4(b)** shows the PL image of our institution names within an area of 57 x 57 μm^2 and a power density of 5 W/cm^2 using a 20x (0.45 NA) objective lens. The sites inside a single letter are separated by 1.25 µm with the same hole size of 150 nm. **Figure 4(c)** shows the SEM pictures corresponding to the characterized pattern showing the position of the QDs. We attempted to measure the anti-bunching properties from the deposited single QDs using confocal microscopy technique. However, we observed blinking and quenching of the emission, which hindered the proper $g^{(2)}$ measurement with the current emitter.

Table 1 lists existing methods for QDs deterministic positioning. In general, the electrostatic interaction method gives the best single-particle yield, given the fact that the material choices of traps/substrates/QDs are not flexible enough for potential photonic integration. The doctor blade-like technique is also competitive in the yield while the complexity of the method limits its applications. Drop-casting method for deterministic positioning is very straightforward which involves controls in evaporation process, i.e., rate and particle flux, and wetting properties, i.e., contact angle and capillary force, of the solvent to regulate the film formation over the substrate with various dispersed particle, i.e., semiconductor[31,35], oxide[30], metal[46], and polymeric[47]. Compared to the other method, our describe method regulates both the evaporation process and wetting properties in a single setup without additional steps in the preparation of the colloidal solution.

We also observe that the trap/particle size ratio is about 1 – 2 for the electrostatic interaction method, while the ratio is around 2 – 4 for the capillary force method to achieve high single-particle yield. It can be a potential advantage which relaxes the patterning and alignment restriction. Amongst all, the drop-casting method offers easy and fast implementation especially for photonic integration, even though the single-particle yield is low compared to the other classes of method. Comparing to others, we have achieved ~40% single-particle yield from a ~80% site occupancy in a single step. Yet, there is a need to explore the possibility achieving a sub-Poissonian distribution for QDs, surpassing the ~37% limit imposed by the Poissonian distribution, which may require engineering the surface properties of the colloids.

Table 1. List of the deterministic positioning methods of QDs. Optimal yield is based on the highest single-particle yield. (*) indicating yield counted from different size variation.

Ref	Method		QDs Description			Template Description				Optimal Yield			
	Main Method	Additional Method	Material	Solvent	Diameter	Substrate	Trap Size		Lift-Off	Single	Total	Trap/QD Lateral Size Ratio	Total Sites Count
							Lateral	Vertical					
This work	Drop Casting	Dried within saturated ethanol vapor	CdSe/CdS/ CdZnS@SiO_2	Water	35 nm	PMMA hole on Si	130 - 150 nm	60 nm	Yes	40%	80%	3.7	393
30	Drop Casting	Mix ethanol into water QDs	CdSe/CdS @SiO_2	Water	35 nm	PMMA hole on ITO	100 nm	25 nm	No	32%	60%	2.9	200
31	Drop Casting	Dried within saturated acetone vapor	CdSeTe/ZnS	Decane	-	PMMA hole on Si	50 nm	135 nm	Yes	28%	32%	-	25
35	Drop Casting/Spin Coating	-	CdSe	Hexane	6 nm	PMMA hole on Si	8 – 15 nm	12 nm	Yes	6% (*)	87% (*)	-	54
33	Langmuir Blodgett	-	CdSe/CdS	Toluene	13 nm	ZEP hole on Si	31.6 - 46.8 nm	33 nm	Yes	40%	70%	2.4	300
22	Doctor Blade-Like	-	CdSe/CdS @SiO_2	Water	90 nm	PMMA hole on Si/SiO_2	122 - 238 nm	157 nm	Yes	75% (*)	89% (*)	-	216
29	Doctor Blade-Like	-	NV Center Nanodiamond	Water	40 nm	PMMA hole on Si/SiO_2	35 - 48 nm	62 nm	Yes	-	75% (*)	-	3380
34	Doctor Blade-Like	Electrostatic interaction from heterogeneous template	CdSe	Water	10 nm	PPA/PMMA/ MA hole on ITO	120 nm	60 nm	No	57%	-	12	781
28	Electrostatic Interaction	-	CdSe/ZnCdS /ZnS@SiO_2	Ethanol	220 nm	PDDA patch on SiO_2	200 - 400 nm	-	No	95%	95%	1.1	-
27	Electrostatic Interaction	-	CdSe/ZnCdS /ZnS@SiO_2	Ethanol	160 nm	Al_2O_3, Y_2O_3, MgO patch on SiO_2	160 nm	20 nm	No	100%	100%	1	-
			Nanodiamonds	Ethanol	40 nm	Al_2O_3 patch on SiO_2	70 nm	20 nm	No	48%	-	1.8	-

Conclusions

In this study, we described a method of saturated ethanol vapor drop casting in which we demonstrate high sites occupancy with optimum single-particle yield following the Poissonian distribution. We employed silica shells to effectively increase the size of the quantum dots (QDs), thereby simplifying template fabrication by accommodating larger trap sizes prepared with EBL process. Additionally, the silica coating facilitated phase transfer to water as a solvent and conferred versatility for broader applications across various core material classes. Utilizing a water/ethanol-vapor setup, we promoted large-area, uniform mass deposition to ensure high reproducibility. This setup also reduced the contact angle, enhancing capillary force at the contact pinning region. As a result, our approach offers a straightforward solution without requiring complex setups or extensive optimization. Finally, our approach of assembling silica-coated QDs holds promise for extending to other classes of core nanoparticles, enabling deterministic patterning within complex photonic platforms with a simple process and setup.

Author Contributions

# (MTP and DA) These authors contributed equally. MTP, DA, JKWY, and DL designed the experiments. XL synthesized silica-coated QDs under HVD supervision. MTP and DA conduct the experiment and analyze data. BS, MRC, CNV, GZ, and MAR assist in experimental setup optimization. MTP and DL collect PL data measurement. ASR collects contact angle data measurement. The initial manuscript was written by MTP and DA, then reviewed and revised by MRC, NVC, JKWY, and DL with the assistance from all authors.

Conflicts of interest

There are no conflicts to declare.

Acknowledgements

This work was supported by the A*STAR MTC Programmatic grant No. M21J9b0085 and MTC Individual Research Grants (IRG) grant No. M22K2c0090. MTP thanks for the support from the A*STAR Singapore International Graduate Award (SINGA) Scholarship. HVD gratefully acknowledges support from TÜBA.

References

1 L. S. Madsen, F. Laudenbach, M. F. Askarani, F. Rortais, T. Vincent, J. F. F. Bulmer, F. M. Miatto, L. Neuhaus, L. G. Helt, M. J. Collins, A. E. Lita, T. Gerrits, S. W. Nam, V. D. Vaidya, M. Menotti, I. Dhand, Z. Vernon, N. Quesada and J. Lavoie, *Nature*, 2022, **606**, 75–81.

2 H. Wang, J. Qin, X. Ding, M.-C. Chen, S. Chen, X. You, Y.-M. He, X. Jiang, L. You, Z. Wang, C. Schneider, J. J. Renema, S. Höfling, C.-Y. Lu and J.-W. Pan, *Phys. Rev. Lett.*, 2019, **123**, 250503.

3 K. Santhosh, O. Bitton, L. Chuntonov and G. Haran, *Nat Commun*, 2016, **7**, ncomms11823.

4 O. Bitton, S. N. Gupta, L. Houben, M. Kvapil, V. Křápek, T. Šikola and G. Haran, *Nat Commun*, 2020, **11**, 487.

5 M. Nonahal, J. Horder, A. Gale, L. Ding, C. Li, M. Hennessey, S. T. Ha, M. Toth and I. Aharonovich, *Nano Lett.*, 2023, **23**, 6645–6650.

6 A. P. Foster, D. Hallett, I. V. Iorsh, S. J. Sheldon, M. R. Godsland, B. Royall, E. Clarke, I. A. Shelykh, A. M. Fox, M. S. Skolnick, I. E. Itskevich and L. R. Wilson, *Phys. Rev. Lett.*, 2019, **122**, 173603.

7 A. Tiranov, V. Angelopoulou, C. J. van Diepen, B. Schrinski, O. A. D. Sandberg, Y. Wang, L. Midolo, S. Scholz, A. D. Wieck, A. Ludwig, A. S. Sørensen and P. Lodahl, *Science*, 2023, **379**, 389–393.

8 S. J. Masson and A. Asenjo-Garcia, *Nat Commun*, 2022, **13**, 2285.

9 G. Rainò, M. A. Becker, M. I. Bodnarchuk, R. F. Mahrt, M. V. Kovalenko and T. Stöferle, *Nature*, 2018, **563**, 671–675.

10 J. D. Thompson, T. G. Tiecke, N. P. De Leon, J. Feist, A. V. Akimov, M. Gullans, A. S. Zibrov, V. Vuletić and M. D. Lukin, *Science*, 2013, **340**, 1202–1205.

11 S. Deshpande, J. Heo, A. Das and P. Bhattacharya, *Nat Commun*, 2013, **4**, 1675.

12 A. Senichev, S. Peana, Z. O. Martin, O. Yesilyurt, D. Sychev, A. S. Lagutchev, A. Boltasseva and V. M. Shalaev, *ACS Photonics*, 2022, **9**, 3357–3365.

13 T. Heindel, C. Schneider, M. Lermer, S. H. Kwon, T. Braun, S. Reitzenstein, S. Höfling, M. Kamp and A. Forchel, *Applied Physics Letters*, 2010, **96**, 011107.

14 R. Uppu, F. T. Pedersen, Y. Wang, C. T. Olesen, C. Papon, X. Zhou, L. Midolo, S. Scholz, A. D. Wieck, A. Ludwig and P. Lodahl, *Sci. Adv.*, 2020, **6**, eabc8268.

15 K. Ngan, Y. Zhan, C. Dory, J. Vučković and S. Sun, *Nano Lett.*, 2023, **23**, 9360–9366.

16 D. Riedel, H. Lee, J. F. Herrmann, J. Grzesik, V. Ansari, J.-M. Borit, H. S. Stokowski, S. Aghaeimeibodi, H. Lu, P. J. McQuade, N. A. Melosh, Z.-X. Shen, A. H. Safavi-Naeini and J. Vučković, *ACS Photonics*, , DOI:10.1021/acsphotonics.3c00992.

17 Y. Luo, N. Liu, X. Li, J. C. Hone and S. Strauf, *2D Mater.*, 2019, **6**, 035017.

18 S. Bisschop, P. Geiregat, T. Aubert and Z. Hens, *ACS Nano*, 2018, **12**, 9011–9021.

19 H. Lu, G. M. Carroll, N. R. Neale and M. C. Beard, *ACS Nano*, 2019, **13**, 939–953.

20 S. Krishnamurthy, A. Singh, Z. Hu, A. V. Blake, Y. Kim, A. Singh, E. A. Dolgopolova, D. J. Williams, A. Piryatinski, A. V. Malko, H. Htoon, M. Sykora and J. A. Hollingsworth, *ACS Nano*, 2021, **15**, 575–587.

21 F. P. García de Arquer, D. V. Talapin, V. I. Klimov, Y. Arakawa, M. Bayer and E. H. Sargent, *Science*, 2021, **373**, eaaz8541.

22 H. A. Nguyen, D. Sharp, J. E. Fröch, Y.-Y. Cai, S. Wu, M. Monahan, C. Munley, A. Manna, A. Majumdar, C. R. Kagan and B. M. Cossairt, *ACS Appl. Mater. Interfaces*, 2023, **15**, 4294–4302.

23 H.-W. Huang, P. Bhadrachalam, V. Ray and S. J. Koh, *Applied Physics Letters*, 2008, **93**, 073110.

24 L. Jiang, W. Wang, H. Fuchs and L. Chi, *Small*, 2009, **5**, 2819–2822.

25 M. Asbahi, S. Mehraeen, F. Wang, N. Yakovlev, K. S. L. Chong, J. Cao, M. C. Tan and J. K. W. Yang, *Nano Lett.*, 2015, **15**, 6066–6070.

26 H. Utzat, W. Sun, A. E. K. Kaplan, F. Krieg, M. Ginterseder, B. Spokoyny, N. D. Klein, K. E. Shulenberger, C. F. Perkinson, M. V. Kovalenko and M. G. Bawendi, *Science*, 2019, **363**, 1068–1072.

27 M. Jiang, J. A. Kurvits, Y. Lu, A. V. Nurmikko and R. Zia, *Nano Lett.*, 2015, **15**, 5010–5016.
28 Q. Zhang, C. Dang, H. Urabe, J. Wang, S. Sun and A. Nurmikko, *Opt. Express*, 2008, **16**, 19592.
29 H. J. Shulevitz, T.-Y. Huang, J. Xu, S. J. Neuhaus, R. N. Patel, Y. C. Choi, L. C. Bassett and C. R. Kagan, *ACS Nano*, 2022, **16**, 1847–1856.
30 M. Barelli, C. Vidal, S. Fiorito, A. Myslovska, D. Cielecki, V. Aglieri, I. Moreels, R. Sapienza and F. Di Stasio, *ACS Photonics*, 2023, **10**, 1662–1670.
31 A. Eich, T. C. Spiekermann, H. Gehring, L. Sommer, J. R. Bankwitz, P. P. J. Schrinner, J. A. Preuß, S. Michaelis De Vasconcellos, R. Bratschitsch, W. H. P. Pernice and C. Schuck, *ACS Photonics*, 2022, **9**, 551–558.
32 M. Kosmulski, *Chemical Properties of Material Surfaces*, CRC Press, Boca Raton, 2001.
33 W. Xie, R. Gomes, T. Aubert, S. Bisschop, Y. Zhu, Z. Hens, E. Brainis and D. Van Thourhout, *Nano Lett.*, 2015, **15**, 7481–7487.
34 G. Cheng, Z. Wang, Z. Man, Y. Meng, M. Chen, J. Bian, Z. Lu and W. Zhang, *ACS Appl. Nano Mater.*, 2022, **5**, 5756–5763.
35 V. R. Manfrinato, D. D. Wanger, D. B. Strasfeld, H.-S. Han, F. Marsili, J. P. Arrieta, T. S. Mentzel, M. G. Bawendi and K. K. Berggren, *Nanotechnology*, 2013, **24**, 125302.
36 H. Hu and R. G. Larson, *J. Phys. Chem. B*, 2006, **110**, 7090–7094.
37 M. Majumder, C. S. Rendall, J. A. Eukel, J. Y. L. Wang, N. Behabtu, C. L. Pint, T.-Y. Liu, A. W. Orbaek, F. Mirri, J. Nam, A. R. Barron, R. H. Hauge, H. K. Schmidt and M. Pasquali, *J. Phys. Chem. B*, 2012, **116**, 6536–6542.
38 H. Kim, F. Boulogne, E. Um, I. Jacobi, E. Button and H. A. Stone, *Phys. Rev. Lett.*, 2016, **116**, 124501.
39 F. Zhang, Z.-F. Shi, Z.-Z. Ma, Y. Li, S. Li, D. Wu, T.-T. Xu, X.-J. Li, C.-X. Shan and G.-T. Du, *Nanoscale*, 2018, **10**, 20131–20139.
40 S. Liu and M.-Y. Han, *Chemistry – An Asian Journal*, 2010, **5**, 36–45.
41 E. Ureña-Horno, M.-E. Kyriazi and A. G. Kanaras, *Nanoscale Advances*, 2021, **3**, 3522–3529.
42 R. D. Deegan, O. Bakajin, T. F. Dupont, G. Huber, S. R. Nagel and T. A. Witten, *Nature*, 1997, **389**, 827–829.
43 S. Mehraeen, M. Asbahi, W. Fuke, J. K. W. Yang, J. Cao and M. C. Tan, *Langmuir*, 2015, **31**, 8548–8557.
44 Z. Luo and S. Mehraeen, *ACS Appl. Nano Mater.*, 2023, **6**, 283–295.
45 Z. Luo and S. Mehraeen, *Mol. Syst. Des. Eng.*, 2023, **8**, 1075–1086.
46 F. Fan and K. J. Stebe, *Langmuir*, 2004, **20**, 3062–3067.
47 H. Kadiri, S. Kostcheev, D. Turover, R. Salas-Montiel, K. Nomenyo, A. Gokarna and G. Lerondel, *Beilstein J. Nanotechnol.*, 2014, **5**, 1203–1209.